37th European Rotorcraft Forum
September 13–15, 2011, Ticino Park, Italy

145
An Experimental Set Up for the Study of the Retreating Blade Dynamic Stall

Alex Zanotti*, Franco Auteri, Gabriele Campanardi and Giuseppe Gibertini

Dipartimento di Ingegneria Aerospaziale – Politecnico di Milano
Via La Masa 34, 20156 Milano – Italy
e–mail: *zanotti@aero.polimi.it

Abstract

In the aim of research about retreating blade dynamic stall control for helicopter performance improvement, a new experimental rig has been designed consisting in a blade section model supported by a motorized strut that can move it in pitch around its quarter chord. The design and performance of the experimental rig have been purposely conceived to reproduce the deep dynamic stall condition of a full-scale retreating rotor blade section at 75% radius at high forward flight speed, in order to test real control systems of the dynamic stall phenomenon on helicopter blade sections. Several measurement techniques as, for instance, fast unsteady pressure measurements, hot wire anemometer and Particle Image Velocimetry (PIV), can be employed to completely characterise the time dependent flowfield.
The paper describes the first series of experiments carried out on a NACA 23012 blade section to validate the rig performance and the measurements set up. The analysis of the comprehensive data set enabled to complete the description of the dynamic stall phenomenon for the NACA 23012 airfoil and can be suitable to be taken as a reference to validate CFD tools. After the validation tests, the experimental rig will enable to test real control systems of the dynamic stall phenomenon on helicopter blade sections.

1 Introduction

The investigation of the dynamic stall phenomenon on the rotor retreating blade remains a major research topic in helicopter aerodynamics, due to the strong demand for faster helicopters [1]. In fact, many recent experimental activities analysed the effectiveness of different control systems integrated on blade section to mitigate the dynamic stall effects on helicopter performance and expand the flight envelope and vehicle utility. Currently, improvements to control rotor blade dynamic stall rely upon the optimization of the blade airfoil shape, introducing, for example, a variable droop leading edge [3]. Moreover, the use of blowing devices as air-jet vortex generators [4] or plasma actuators [5] represents an attractive solution for the reduction of the airloads hysteresis and the suppression of stall flutter occurrence during a blade pitching cycle [6].
In the aim of testing new flow control devices integrated on real helicopter blade sections, a new experimental activity started at Politecnico di Milano on this topic. The preliminary stage consisted in the validation of a new test apparatus designed for reproducing the dynamic stall condition of a full scale pitching blade section. The paper describes the first series of tests carried out on a NACA 23012 blade section to validate the rig performance and the measurements set up. The NACA 23012 has been selected since, being a typical helicopter blade airfoil, it has been employed in experimental activities in the past years about the study of the dynamic stall phenomenon on pitching blade sections [7, 8]. The

main goal of the validation activity has been to achieve a complete data set in the different regimes of blade dynamic stall described in literature [1] by means of several measurement techniques involved as unsteady pressure measurementsand P.I.V.

2 Experimental set up

The experimental activity was conducted at Politecnico di Milano in the low-speed closed-return wind tunnel of the Aerodynamics Laboratory. The wind tunnel has a rectangular test section with 1.5 m height and 1 m width. The maximum wind velocity is 55 m/s and the turbulence level is less than 0.1%.
The dynamic stall rig has been designed consisting in a blade section model supported by a motorized strut that can move it in pitch around its quarter chord, as can be seen in the layout in Fig.1.

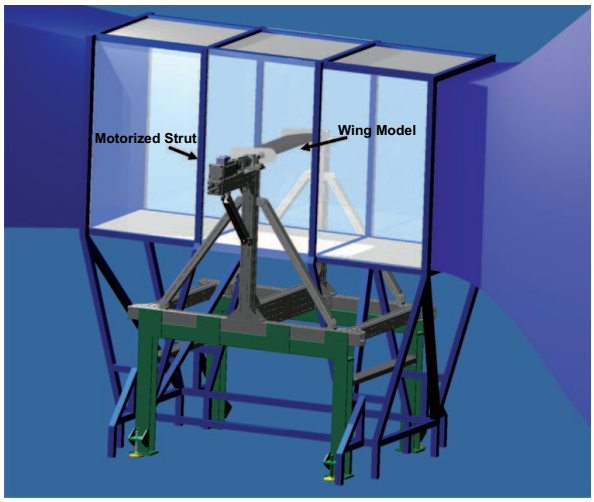

Figure 1: Dynamic stall rig layout in the wind tunnel.

The employed NACA 23012 blade section model, with airfoil chord of 0.3 and aspect ratio of 3.1, was mounted horizontally in the wind tunnel test section and was pivoted about the quarter-chord position on two tubular steel shafts positioned on two self-aligning bearings, see Fig. 2.

The blade section model is composed by three aluminium machined external sections attached on an internal metallic frame in aluminium. The model presents an interchangeable midspan section for the different measurements techniques employed; in particular two central sections were constructed, one for PIV flow surveys and another for unsteady pressure measurement equipped with pressure ports positioned along the midspan chord line. End plates were used during the tests to minimize interference effects of the walls boundary layer. The model was installed on a heavy metallic supporting structure composed by steel beams and aluminium profiles on which were connected the tubular shafts.

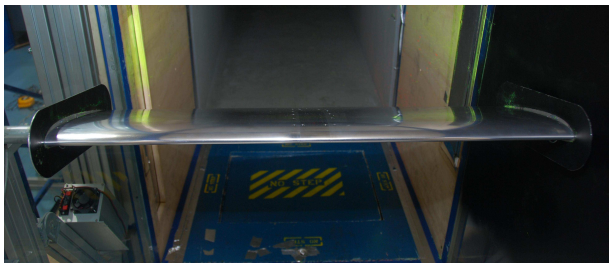

Figure 2: NACA 23012 blade section model inside the wind tunnel.

The blade model pitching motion is driven by a brushless servomotor with a 12:1 gear drive, as can be seen in the particular of the motorized strut in Fig.3. The driving mechanism arrangement is positioned on a cantilevered aluminium profile and provides 120 Nm of continuous torque. The model in connected to the driving mechanism by a torsionally stiff steel laminae coupling between the model tubular shaft and the gear drive shaft. An interface software implemented in **Labview** controls the model pitching sinusoidal motion and the pitching cycle parameters, for instance the mean angle of attack, the amplitude and the oscillation frequency. A 4096 imp/rev encoder is used to determine the instantaneous position of the model as well as for feedback control.

2.1 Unsteady pressure measurement setup

The midspan chord line of the model central section is instrumented with 21 **Kulite** unsteady pressure transducers with a slight increase in concentration near the leading edge. Table 1 presents the positions of the surface pressure ports starting from the leading edge

Figure 3: Particular of the motorized strut.

and following a closed loop from the upper to the lower surface of the airfoil.

#	x/c	#	x/c	#	x/c
1	0	8	0.453	15	0.459
2	0.01	9	0.618	16	0.373
3	0.044	10	0.76	17	0.285
4	0.096	11	0.9	18	0.185
5	0.164	12	0.9	19	0.118
6	0.28	13	0.767	20	0.06
7	0.358	14	0.628	21	0.02

Table 1: Pressure ports location on the model midspan section.

Each pressure transducer is positioned in a straight or L-shaped nylon machined pipe and sealed with a miniature rubber o-ring. Figure 4 presents the particular of the central section of the model instrumented with the pressure transducers.

The pressure signals acquisition was carried out using a **National Instruments** compact data acquisition system **cDAQ-9172** equipped with six **NI 9237** 24 bit simultaneous bridge

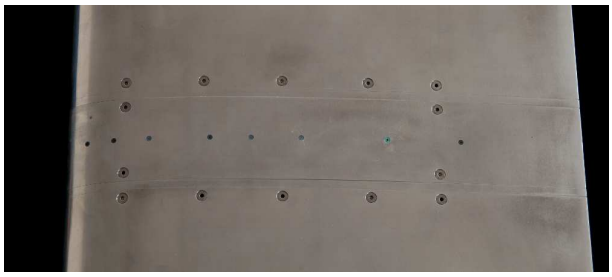

Figure 4: Particular of the model central section instrumented with the pressure transducers.

modules. The trasducers signals were acquired with 50 kHz simultaneous sampling rate on 21 channels for a time period corresponding to 30 complete pitching cycles. The high sampling rate was suggested to capture the fine detail of the dynamic stall phenomenon characterised by severe unsteadiness conditions, especially at the relatively high reduced frequency tested $k = 0.1$. The phase average and the integration of the unsteady pressure measurements obtained from the 21 miniature pressure transducers allowed to determine the time history of airloads, lift and pitching moment, in a pitching cycle and to evaluate its hysteresis.

2.2 PIV setup

A **Pixelfly** double shutter CCD camera with a 12 bit, 1280×1024 pixel array and a 55 mm **Nikon** lens were used to acquire the image pairs. In order to perform the flow survey above the entire airfoil upper surface, the measurement field was composed by 4 measurement windows spanning the airfoil chord direction. The CCD camera was mounted on a dual axis traversing system composed by two stepper motors that allowed to move the measurement window along two orthogonal directions. The PIV system used a **Dantec Dynamics** Nd:Yag double pulsed laser with 200 mJ output energy and a wavelength of 532 nm. The laser sheet passed through an opening in the wind tunnel roof aligned with the flow and positioned in the midspan of the test section width. The laser was mounted on a single axis traversing system to move the sheet along the wind tunnel flow direction, enabling the use of a smaller width sheet with higher energy cen-

tered on the measurement window.
The laser and the camera were mounted on a external metallic structure made of aluminium profiles that was connected to the heavy basement in order to avoid the transfer of the wind tunnel vibrations to the PIV measurement devices during the tests at high speed. Figure 5 presents the arrangement of the PIV devices in the wind tunnel test section.

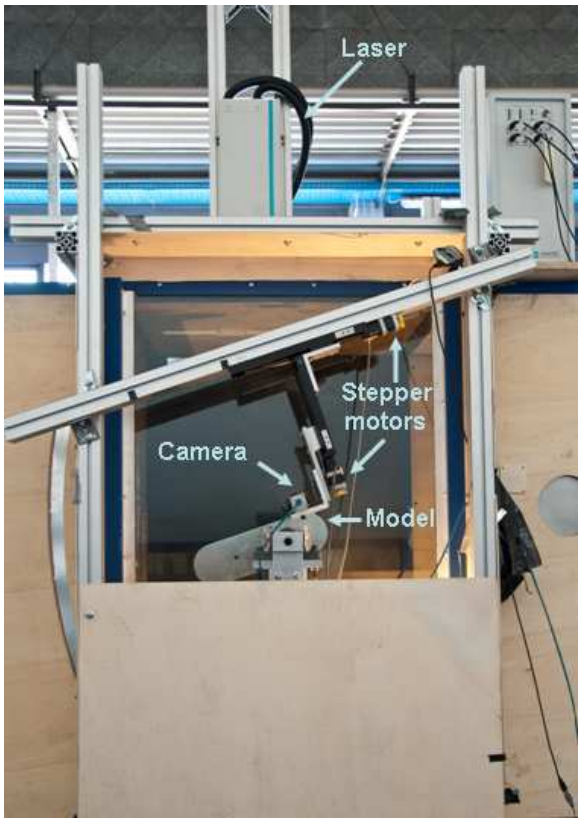

Figure 5: PIV setup in the wind tunnel test section.

The tracer particles injected in the wind tunnel are small oil droplets with diameter in the range of $1-2\ \mu m$, generated by means of Laskin nozzles.

3 Experimental results

3.1 Unsteady pressure measurements

The main objective of the unsteady pressure measurements on the blade section has been the evaluation of the airfoil performance under different pitching cycle conditions, typical of the flight envelope of a helicopter rotor in forward flight. In this aim, the pitching cycles parameters of the performed tests, mean angle of attack α_m, oscillation amplitude α_a and reduced frequency k, have been changed systematically in order to analyse the characteristics of the airloads time histories in the regimes described in literature. The tests have been carried out at $Re = 1 \cdot 10^6$ and $Ma = 0.15$ in order to reproduce the condition of a full-scale reatreating rotor blade section at 75% radius in forward flight. A few tests have been carried out also at $Re = 6 \cdot 10^5$ in order to evaluate the effect of Reynolds number on the airloads in dynamic conditions.
Before the dynamic tests, static tests have been carried out at $Re = 1 \cdot 10^6$ in order to validate the airloads measurement technique. The measured $C_L - \alpha$ curve presented in Fig.6 presents a very good agreement with the curve measured by Leishman [7] for NACA 23012 airfoil at $Re = 1.5 \cdot 10^6$. The static airloads are not corrected by the wind tunnel wall effects to better compare them with the dynamic results because well-established correction methods are not available for pitching airfoils.

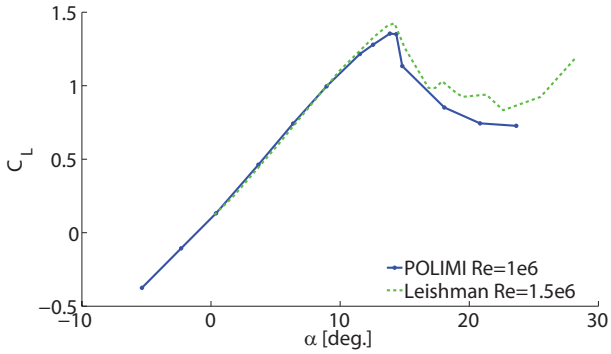

Figure 6: Comparison of steady $C_L - \alpha$ curves for NACA 23012.

3.1.1 *Effect of mean angle of attack*

The effects of mean angle of attack variations have been evaluated reproducing pitching cycles with α_m in the interval between 5° and 20° with a constant oscillation amplitude of 10° and a reduced frequency of 0.1. As can be observed from the tests results presented in Fig.7 the Reynolds effect on the dynamic airloads curves are quite small.
The conditions tested represent the two different regimes described in literature as

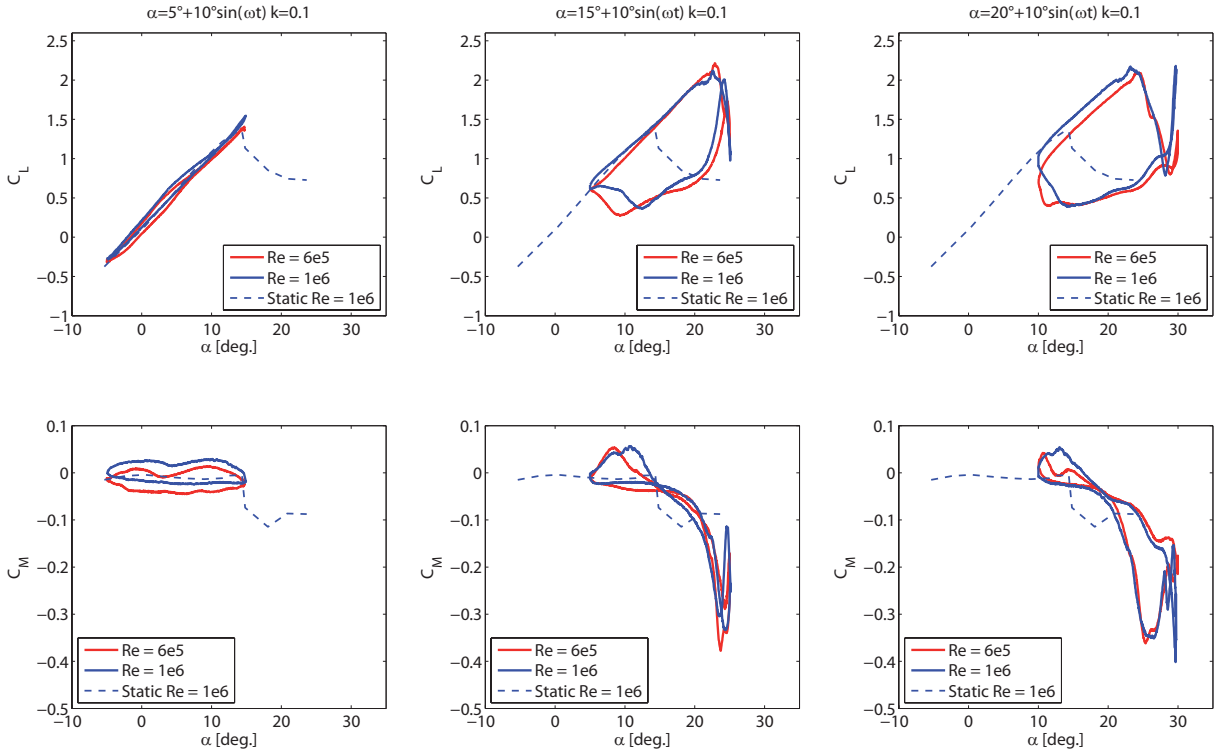

Figure 7: Effects of mean angle of attack variations on lift and pitching moment curves for NACA 23012 at $Re = 6 \cdot 10^5$ and $Re = 1 \cdot 10^6$.

Light Dynamic Stall and *Deep Dynamic Stall* [1, 2]. In particular, in the former regime the maximum angle of attack reached by the airfoil during the sinusoidal oscillation is near the static stall angle of attack. As can be seen from the results of the test with $\alpha_m = 5°$, this regime is characterised by minor flow separation from the airfoil as the flow is almost attached during the pitching cycle and consequently the airloads present a small amount of hysteresis.

The conditions tested with $\alpha_m = 15°$ or $\alpha_m = 20°$ represent the *Deep Dynamic Stall* regime as the maximum angle of attack reached by the airfoil during the sinusoidal oscillation is well above the static stall angle of attack and the oscillation amplitudes are conspicous. This regime is characterised by the vortex-shedding phenomenon and a high amount of airloads hysteresis as, during a larger part of the pitching cycle the flow is separated. In fact, as can be seen from the results of the tests with $\alpha_m = 15°$, the $C_L - \alpha$ and $C_M - \alpha$ curves present high overshoots of lift and pitching moment respect to their static values. Moreover, the $C_L - \alpha$ curve presents a non-linear change of the slope immediately prior to reach the maximum lift due to the formation, migration and shedding of a vortex described in literature as *Dynamic Stall Vortex* (**DSV**). This issue produces a delay between the pitching moment break that occurs at about 20° angle of attack and the pitch stall that occurs at about 23°.

The airloads curves for the test condition with $\alpha_m = 20°$ present a quite interesting behavior; in fact, it is possible to notice a secondary peak near the end of the upstroke motion of the airfoil. This behavior is explained by the formation of a second vortex disturbance that moves on the upper surface of the airfoil. The phenomenon of formation and convection of two vortex for this test condition is clearly visible in Fig.8 that shows the time history of the pressure coefficient C_P on the airfoil upper surface during the pitching cycle. The primary vortex disturbance starts at about 22° angle of attack and produces a divergence of pressure at the airfoil trailing

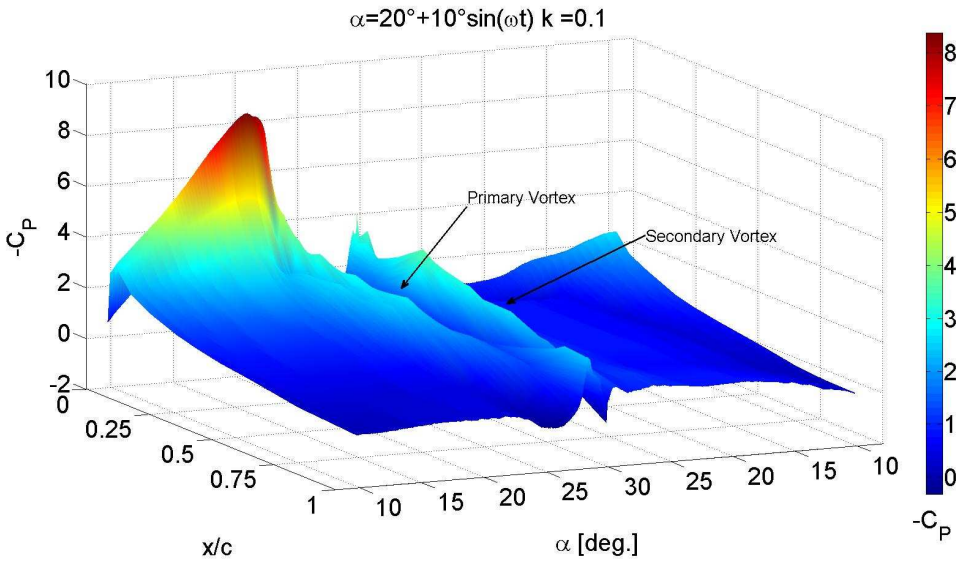

Figure 8: Pressure coefficient time history on the airfoil upper surface in *Deep Dynamic Stall* condition at $Re = 1 \cdot 10^6$.

edge as it moves over the chord. The secondary vortex disturbance appears near the maximum angle of attack at about 28° angle of attack and produces a pressure wave that convects faster than the primary over the chord.

In Fig.9 the dynamic airloads curves measured for two conditions at $Re = 1 \cdot 10^6$ are compared with the curves from Leishman [7] at $Re = 1.5 \cdot 10^6$. For the test condition with $\alpha_m = 6°$ the airloads curves are in good agreement while for the test condition with $\alpha_m = 20°$, characterised by very high angles of attack, the curves presents a sensibly different behavior. Although the different Reynolds number has to be considered, the most of the differences between the present results and the reference work of Leishman could be due to some differences in the two set up and namely to the different wind tunnel blockage (that is larger in Leishman's tests).

3.1.2 *Effect of reduced frequency*

The effects of reduced frequency variations have been evaluated reproducing pitching cycles with k in the interval between 0.05 and 0.1 with a constant mean angle of attack and oscillation amplitude of 10°. The tests results are presented in Fig.10. The effect of the reduced frequency increase is the delay of the onset of flow separation at a higher angle of attack that produces a reduction of the airloads overshoots and hysteresis. This effect can be explained by the increase of a kinematic induced camber effect due to the rapid pitching motion of the airfoil that decreases the pressure gradients over the chord for a certain lift value [2]. Moreover, the increasing reduced frequency produces also the delay of the onset of secondary vortex formation.
As can be observed from Fig.10, the $C_M - \alpha$ curves for the higher reduced frequencies tested present clockwise loop corresponding to negative aerodynamic torsional damping; this condition could lead to the occurrence of an aeroelastic instability described in literature as *Stall Flutter* [6].

3.2 PIV flow surveys

This section presents the results of the PIV flow surveys carried out above the upper surface of the pitching airfoil in regime of *Deep Dynamic Stall*. In particular the selected motion condition of the airfoil was:

$$\alpha(t) = 15 + 10sin(\omega t) \qquad (1)$$

with a reduced frequency $k = 0.1$. The wind tunnel velocity for PIV surveys was 30 m/s corresponding to $Re = 6 \cdot 10^5$ and $Ma = 0.088$.

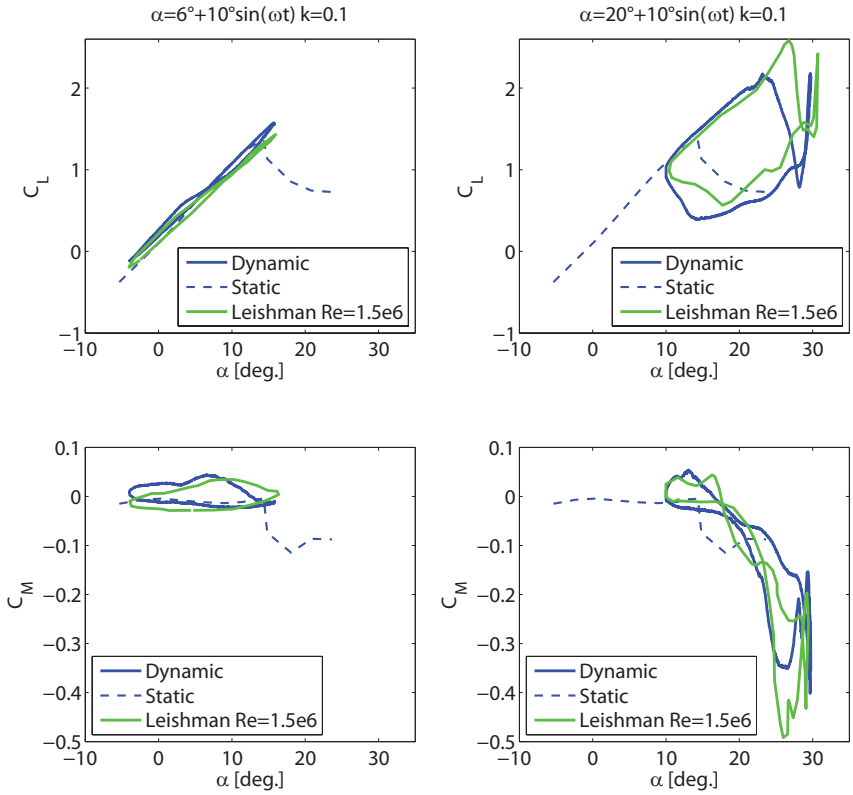

Figure 9: Comparison of the dynamic airloads curves for NACA 23012 at $Re = 1 \cdot 10^6$ with Leishman [7].

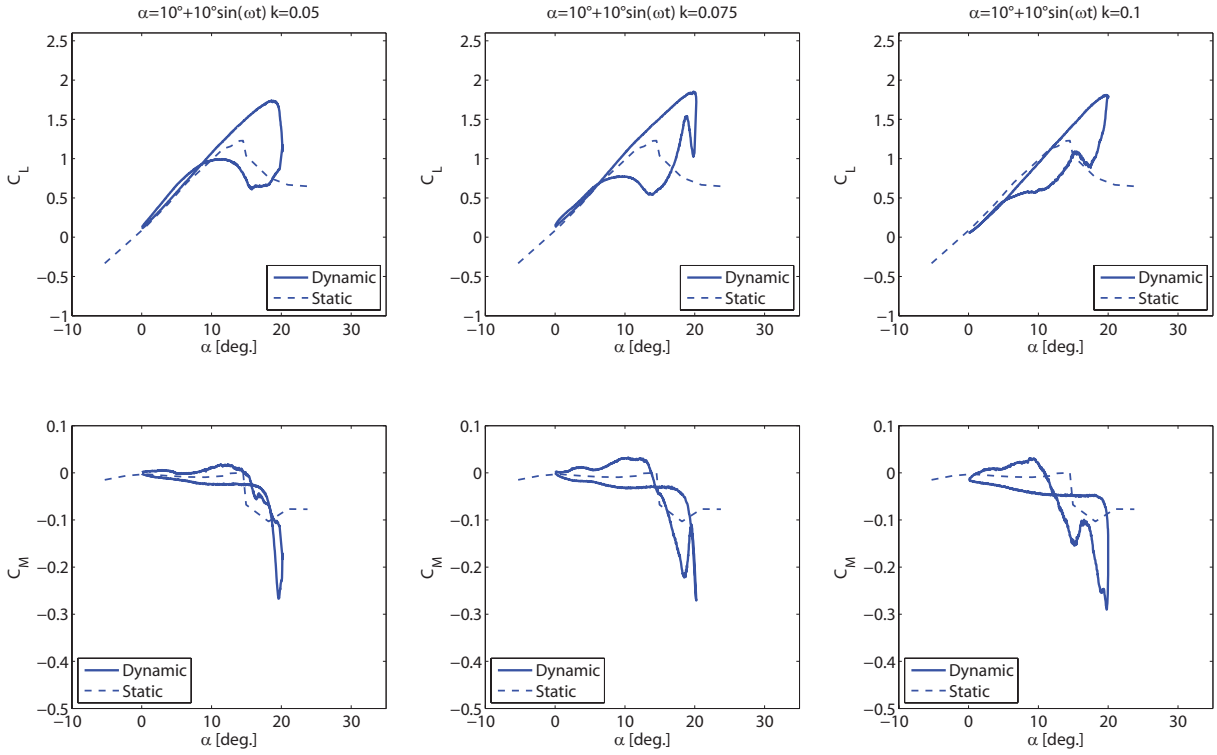

Figure 10: Effects of reduced frequency variations on lift and pitching moment curves for NACA 23012 at $Re = 1 \cdot 10^6$.

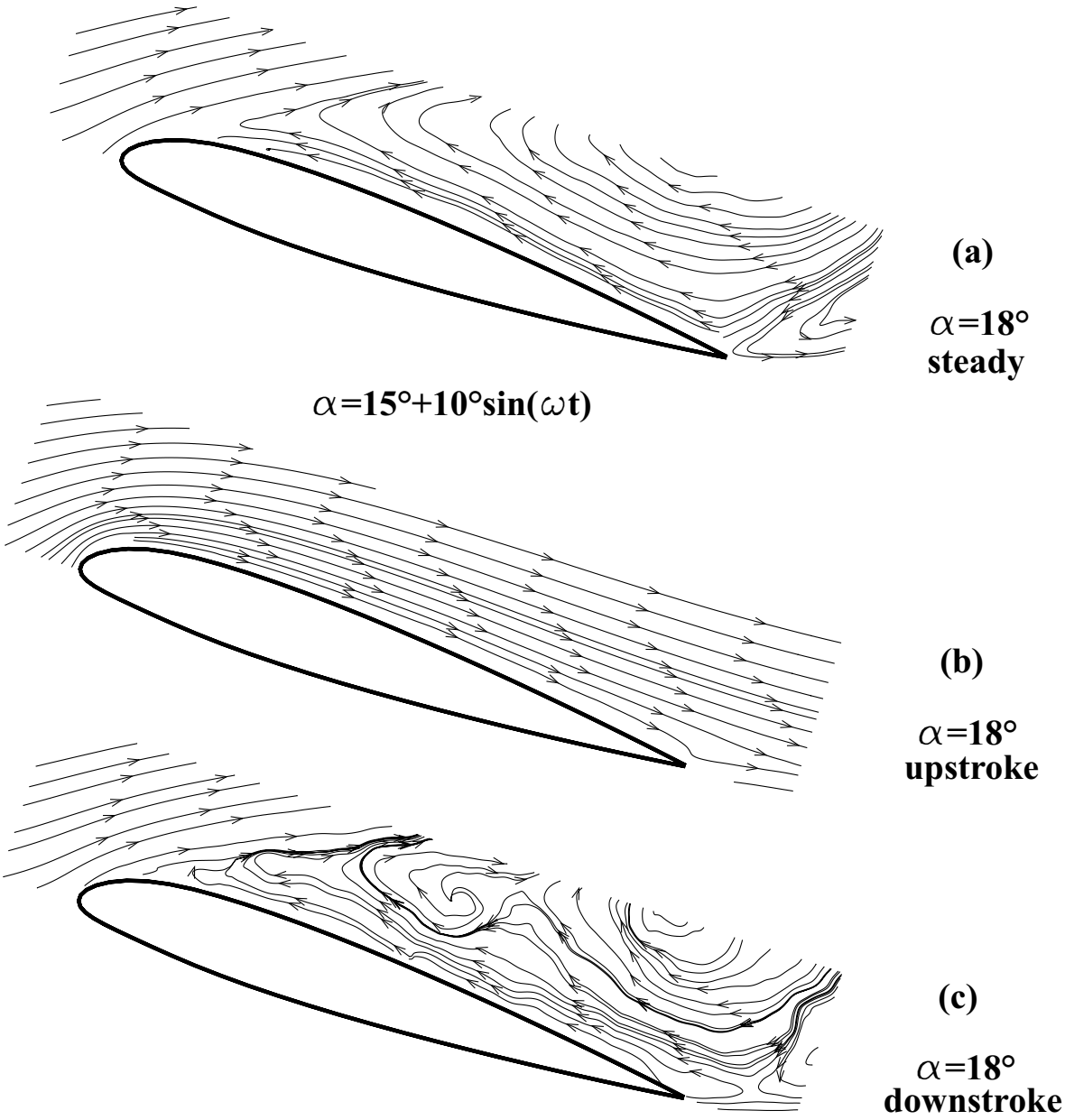

Figure 11: Steady and unsteady PIV flow surveys for NACA 23012 at $\alpha = 18°$ and $Re = 6 \cdot 10^5$.

The main goal of the PIV flow surveys was to describe the flow physics of the blade dynamic stall under severe unsteadiness conditions and in particular the main events that characterise the phenomenon. In the following figures the measured velocity flow fields are presented by the istantaneous streamlines.
In order to point out the differences between the steady and the unsteady flow field, a preliminary PIV survey in static condition has been carried out for the airfoil at $\alpha = 18°$ corresponding to a post-stall condition. Figure 11 presents the comparison between the flow fields measured at the same incidence of 18° in steady case and in the unsteady oscillating condition described by Eq. 1 both in upstroke and downstroke. The steady case at $\alpha = 18°$ in post-stall condition, see Fig. 11(a), presents a separated flow starting from the leading edge of the airfoil while in the unsteady condition for upstroke motion at the same incidence the flow is fully attached, see Fig. 11(b).

Consequently, the different flow fields measured in steady and unsteady condition shows

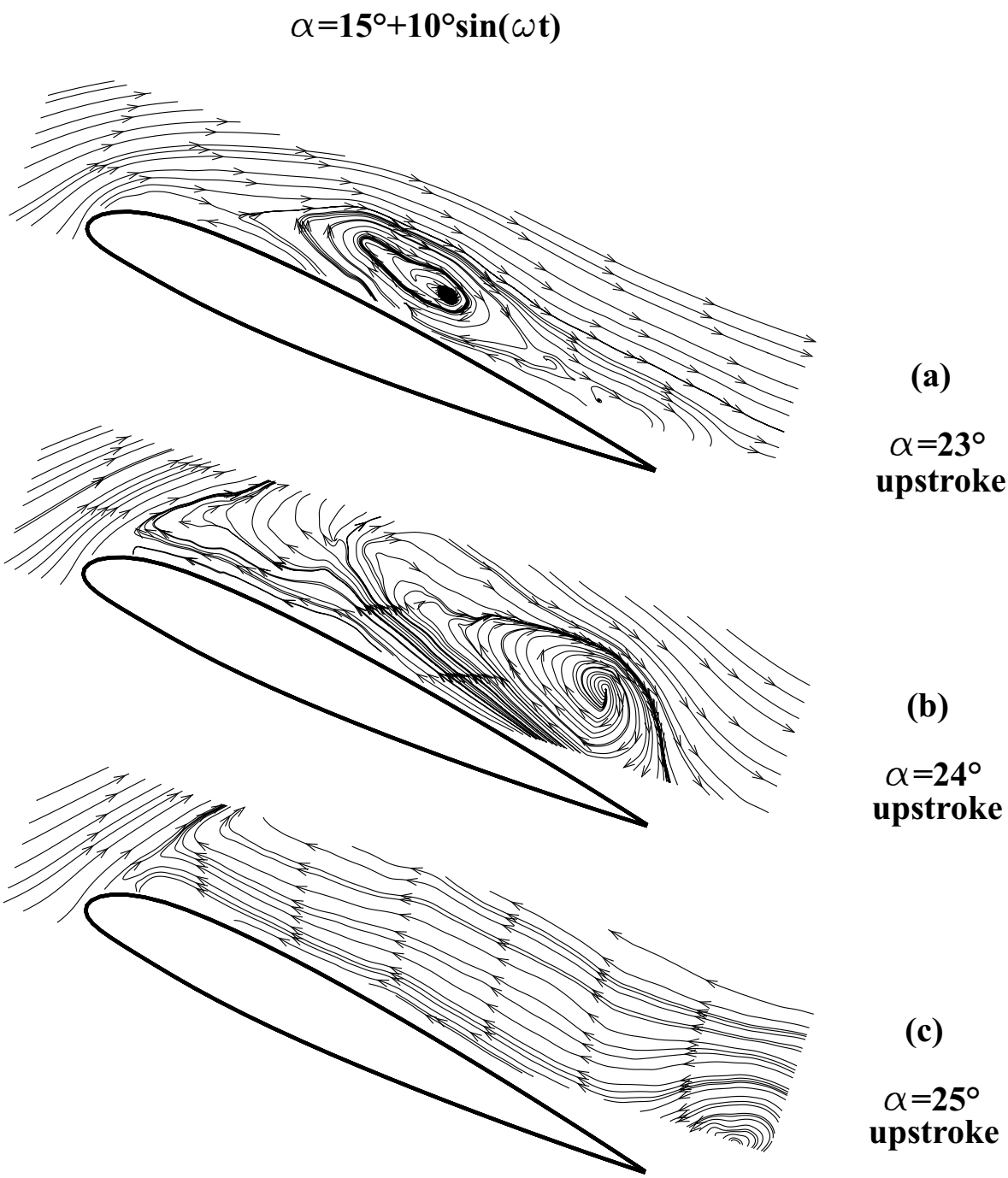

Figure 12: Unsteady PIV flow surveys for NACA 23012 at $Re = 6 \cdot 10^5$ in Deep Dynamic Stall condition.

one of the main features of the dynamic stall phenomenon that is the delay of stall to higher incidences.

Moreover, as can be observed from Fig. 11(c), the flow topology at $\alpha = 18^\circ$ during the motion of downstroke presents a wide separation above the upper surface of the airfoil with strong vortical structures. The different behavior of the flow topology during the motion of upstroke and downstroke explains the asymmetry of the airloads with respect to the motion of the body during the pitching cycle that produces a large amount of airloads hysteresis.

Figure 12 presents the flow fields measured at higher incidences in the unsteady oscillating condition described by Eq. 1 and illustrates

the main feature of the *Deep Dynamic Stall* regime consisting in the formation at the airfoil leading edge and migration above the airfoil upper surface of the dynamic stall vortex. As can be observed from Fig. 12)(a), the dynamic stall vortex reach the airfoil midchord at $\alpha = 23°$ and presents a clockwise rotation; at the higher incidence of $\alpha = 24°$, the vortex grows and moves downstream (see Fig. 12(b)) up to shed from the trailing edge at the maximum incidence of the oscillating cycle, $\alpha = 25°$, where the airfoil reverses the pitching motion (see Fig. 12(c)).

4 Conclusions

The performance of the new experimental rig designed for the study of the retreating blade dynamic stall has been validated demonstrating great reliability also for the wind tunnel tests that reproduced the deep dynamic stall regime of a full-scale retreating rotor blade section at high forward flight speed. The experimental techniques employed in the first wind tunnel tests campaign enabled to complete the description of the typical issues involved in the phenomenon for the NACA 23012 airfoil, demonstrating a good choice of the measurement set up. In particular the unsteady pressure measurements allowed to evaluate the different amount of the airloads hysteresis in the regimes described in literature, while the PIV flow field surveys performed with a high spatial resolution showed the flow physics of the blade stall under the severe unsteadiness condition of the *Deep Dynamic Stall* regime.
The comprehensive data set produced by the measurement techniques could be considered a good data base for the validation of CFD tools. After the preliminary validation activity of the performance and set up of the measurement techniques, the experimental rig will be soon employed to test real control systems of the dynamic stall phenomenon integrated on blade section models, as for example self-activated movable flaps and Gurney flaps, in order to evaluate their capability to reduce the amount of the airload hysteresis during the pitching cycle and improve the rotor performance.

References

[1] W.J. McCroskey. The Phenomenon of Dynamic Stall, NASA TM 81264, 1981.

[2] J.G. Leishman. Principles of helicopter aerodynamics, Cambridge Aerospace Series, 2000.

[3] M. Chandrasekhara, P. Martin and C. Tung. Compressible Dynamic Stall Control Using a Variable Droop Leading Edge Airfoil, *Journal of Aircraft*, **41**, 862-869, 2004.

[4] C. Singh, D. Peake, A. Kokkalis, V. Khodagolian, F. Coton and R. Galbraith. Control of Rotorcraft Retreating Blade Stall Using Air-Jet Vortex Generators, *Journal of Aircraft*, **43**, 1169-1176, 2006.

[5] M. Post and T. Corke. Separation Control Using Plasma Actuators: Dynamic Stall Vortex Control on Oscillating Airfoil, *AIAA Journal*, **44**, 3125-3135, 2006.

[6] F.O. Carta. An Analysis of the Stall Flutter instability of Helicopter Rotor Blades, *Journal of American Helicopter Society*,**12**, 1-8, 1967.

[7] J.G. Leishman. Dynamic stall experiments on the NACA 23012 aerofoil, *Experiments in Fluids*, **9**, 49-58, 1990.

[8] M. Raffel, J. Kompenhans, B. Stasicki, B. Bretthauer and G.E.A. Meier. Velocity measurement of compressible air flows utilizing a high-speed video camera, *Experiments in Fluids*, **18**, 204-206, 1995.